David Tomás Sánchez Martínez
Lourdes García Rodríguez
(coordinadores)

Proceedings of the 7th International Seminar on ORC Power Systems

Editorial Universidad de Sevilla

Proceedings of the 7th International Seminar on

ORC
Power Systems

David Tomás Sánchez Martínez
Lourdes García Rodríguez
(coordinadores)

Proceedings of the 7th International Seminar on

ORC Power Systems

(ORC2023)

4th to 6th
SEPTEMBER
SEVILLE 2023

EDITORIAL UNIVERSIDAD DE SEVILLA

Sevilla, 2024

Colección Actas
Núm.: 91

ISBN 978-84-472-2745-7
DOI: https://dx.doi.org/10.12795/9788447227457

Diseño de cubierta y maquetación: los autores

INDEX OF CONTRIBUTIONS

ID3 - Additive manufacturing for fast prototyping of a velocity compounded radial re-entry turbine
Authors: Dominik Stümpfl, Karel Ráž, Philipp Streit, Andreas P. Weiß 13

ID4 - Thermodynamic concept of a novel recuperative two-phase power cycle process
Authors: Benedikt G. Bederna, Riley B. Barta, Christiane S. Thomas. 23

ID7 - Performance analysis of a 1.5 MW Organic Rankine Cycle in a Carnot battery system for grid balancing services
Authors: Robin Tassenoy, Hannes Van De Velde, Kenny Couvreur, Michel De Paepe, Steven Lecompte 33

ID8 - Calibration of multi-hole probes for measurements in compressible organic vapor flows
Authors: Leander Hake, Stephan Sundermeier, Stefan Aus Der Wiesche, Maximilian Passmann. 43

ID9 - pocketORC: A browser-based calculator for teaching organic Rankine cycle power systems
Authors: Martin White 53

ID10 - Evaluation of existing supercritical heat transfer correlations for designing the vapor generator in low-temperature transcritical Organic Rankine Cycle systems
Authors: Jera Van Nieuwenhuyse, Anastasios Skiadopoulos, Dimitris Manolakos, Steven Lecompte, Michel De Paepe 61

ID12 - A novel combined cooling and power cycle integrated ejector refrigeration and composition adjustment for stationary engine waste heat recovery
Authors: Xiaocun Sun, Lingfeng Shi, Hua Tian, Gequn Shu 71

ID14 - Design and construction of a reversible ORC test rig for geothermal CHP applications
Authors: Florian Kaufmann, Christopher Schifflechner, Christoph Wieland, Hartmut Spliethoff 81

ID15 - Robust and fast meanline methodology for radial inflow turbines with non-ideal gases for system level optimisation of organic Rankine cycles
Authors: Carola Freytag, Eva Alvarez-Regueiro, Pablo Ale-Martos, Esperanza Barrera-Medrano, Ricardo Martinez-Botas. 91

ID16 - Shape optimization of a sCO2 centrifugal compressor stage
Authors: Alessandro Romei, Paolo Gaetani, Giacomo Persico 101

ID17 - Optimizing the performance of a hybrid solar-biomass micro-CHP system with a TFC engine as the prime mover for domestic applications
Authors: Anastasios Skiadopoulos, Xander Van Heule, Steven Lecompte, Michel De Paepe, Dimitrios Manolakos 109

ID19 – Systematic and multi-criteria optimisation of subcritical thermally integrated Carnot batteries (TI-PTES) in an extended domain
Authors: Antoine Laterre, Olivier Dumont, Vincent Lemort, Francesco Contino 119

ID20 - ORC technology used in a heat removal system for an advanced nuclear power plant
Authors: Guillaume Lhermet, Benoit Payebien, Nicolas Tauveron, Nadia Caney, Franck Morin 130

ID22 - Assessment of trilateral Organic Rankine Cycle for solar applications with innovative turboexpander concept
Authors: Alessandro Romei, Andrea Giostri, Andrea Spinelli. 140

ID25 - Evaluation of the performance of an axial one-stage 10kW turbogenerator through experimental testing
Authors: Piotr Klimaszewski, Piotr Klonowicz, Lukasz Witanowski, Tomasz Suchocki, Piotr Lampart, Eugeniusz Ihnatowicz, Lukasz Antczak, Dawid Zaniewski, Lukasz Jedrzejewski 149

ID26 - Investigation of the turbulence level and the vortex shedding in a turbine cascade working with an organic vapor at subsonic Mach numbers
Authors: Leander Hake, Stephan Sundermeier, Stefan Aus Der Wiesche, Camille Matar, Paola Cinnella, Xavier Gloerfelt 159

ID27 - A novel approach to district heating: using a two-phase expander in a reversible heat pump-Organic Rankine Cycle system
Authors: Sindu Daniarta, Attila R. Imre, Piotr Kolasinski 169

ID28 - Optimization of a partially evaporating Organic Rankine Cycle with thermal non-equilibrium expansion
Authors: Xander Van Heule, Tasos Skiadopoulos, Dimitris Manolakos, Michel De Paepe, Steven Lecompte 176

ID29 - Cost-effective option of cold energy utilization in pharmaceutical industry
Authors: Sindu Daniarta, Dawid Sowa, Ádám Havas, Attila R. Imre, Piotr Kolasinski 184

ID30 - Numerical investigation of a transonic dense gas flow over an idealized blade vane configuration
Authors: Aurelien Bienner, Xavier Gloerfelt, Paola Cinnella, Leander Hake, Stefan Aus Der Wiesche 193

ID31 - Comprehensive analysis of ORC-VCC system for air conditioning from low-temperature waste heat
Authors: Lukasz Witanowski 203

ID33 - Pareto front analysis for the design and the working fluid selection in ORC-based pumped thermal energy storage technology in both pure electric and cogenerative applications
Authors: Marco Astolfi, Dario Alfani, Andrea Giostri 214

ID36 - Evaluating the waste heat sources in a very large crude carrier and the potential integration of Organic Rankine Cycle configurations
Authors: Amalia Stainchaouer, Christopher Schifflechner, Christoph Wieland, Hartmut Spliethoff 224

ID37 - Investigating R1234ze and R1234yf as replacements to R134a in waste heat recovery ORC applications
Authors: James Bull, James Buick, Jovana Radulovic 234

ID38 - Performance and economic assessment of a thermally integrated reversible HP/ORC Carnot battery applied to data centers
Authors: Chiara Poletto, Andrea De Pascale, Saverio Ottaviano, Olivier Dumont, Maria Alessandra Ancona, Michele Bianchi 244

ID39 - Evaluation of the performance of multiple supercritical CO2 power cycles in Waste Heat Recovery applications
Authors: Hicham Chibli, Matthew Read, Abdulnaser Sayma 254

ID40 - Design and modeling of a demonstration-scale ORC cycle for the Liquid Air Combined Cycle
Authors: Owen Pryor, William Conlon, Aaron Rimpel, Milton Venetos 264

ID41 - Guidelines and optimization criteria of a machine learning-based methodology for mixture design in ORC systems
Authors: Valerio Mariani, Saverio Ottaviano, Andrea De Pascale, Giulio Cazzoli, Lisa Branchini, Gian Marco Bianchi 273

ID45 - Potential of trigenerative Waste Heat Recovery CO2-mixture transcritical power plants for increasing the sustainability of district heating and cooling networks
Authors: Mattia Baiguini, Michele Doninelli, Ettore Morosini, Dario Alfani, Gioele Di Marcoberardino, Paolo Giulio Iora, GiampaoloManzolini, Constante Mario Invernizzi, Marco Astolfi 282

ID46 - Thermodynamic analysis of a novel pumped thermal energy storage system with waste heat integration
Authors: Meiyan Zhang, Lingfeng Shi, Peng Hu, Gang Pei, Gequn Shu 294

ID48 - Pressure profile optimisation of a nozzle for wet-to-dry expansion
Authors: Pawel Ogrodniczak, Abdulnaser Sayma, Martin T. White 304

ID51 - Thermodynamic modification of CO2-based combined cooling and power cycle with ejector
Authors: Yonghao Zhang, Lingfeng Shi, Gequn Shu 313

ID53 - Selection of suitable working fluid and storage material for ORC coupled with Thermal Energy Storage
Authors: Dawid Sowa, Sindu Daniarta, Piotr Kolasinski 323

ID54 - Influence of dopant fluorination on the heat transfer behaviour of CO2-based mixtures in transcritical power cycles
Authors: Michele Doninelli, Gioele Di Marcoberardino, Costante Mario Invernizzi, Paolo Giulio Iora 333

ID57 - On air-cooled condensers for ORC systems operating with zeotropic mixtures
Authors: Lorenzo Galieti, Carlo De Servi, Dario Alfani, Paolo Silva, Paola Bombarda, Piero Colonna 344

ID58 - Experiments on supersonic ORC nozzles in linear cascade configuration
Authors: Marco Oliveti, Marco Manfredi, Giacomo Persico, Andrea Spinelli, Paolo Gaetani, Vincenzo Dossena 354

ID59 - Numerical analysis of aerodynamics and performance of a radial-inflow micro-ORC turbine
Authors: Fatemeh Ardaneh, Marta Zocca, Antti Uusitalo, Teemu Turunen-Saaresti. 363

ID61 - ORC system using R1233zd(E) for waste heat recovery from the upstream process
Authors: Meng Soon Chiong, Bemgba Nyakuma, Nur Izwanne Mahyon, Srithar Rajoo, Eva Alvarez-Regueiro, Maria Esperanza Barrera-Medrano, Ricardo F. Martinez-Botas, Yossapong Laoonual 373

ID63 - Experimental investigation of a small-scale reversible high temperature heat pump – Organic Rankine Cycle system for industrial Waste Heat Recovery
Authors: Rahul Velanparambil Ravindran, Donal Cotter, Christopher Wilson, Ming Jun Huang, Neil Hewitt. 381

ID64 - Technical comparison and evaluation of a Pumped Thermal Energy Storage with two different designs
Authors: Márcio Santos, Jorge André, Ricardo Mendes, José Ribeiro. 391

ID68 - The potential of CO2-Plume Geothermal (CPG) Systems for CO2 component manufacturers: opportunities and development needs
Authors: Christopher Schifflechner, Jasper De Reus, Hartmut Spliethoff, Martin O. Saar, Sebastian Schuster, Dieter Brillert 400

ID69 - Development of a generalised low-order model for twin-screw compressors
Authors: Florian Kaufmann, Ludwig Irrgang, Christopher Schifflechner, Hartmut Spliethoff. 410

ID71 - Decision-making matrix for the selection of mixture in ORC applications
Authors: William Combaluzier, Nicolas Tauveron, Michel Beaughon, Aldo Serafino 420

ID72 - Reversible heat pump-ORC pilot plant – Experimental results and fluid charge optimization
Authors: Maximilian Weitzer, Sebastian Kolb, Dominik Müller, Jürgen Karl 430

ID73 - Performance of Organic Rankine Cycle system in combination with residual municipal solid waste gasification: a simulation analysis
Authors: Luca Cioccolanti, Giovanni Biancini, Ramin Moradi, Luca Del Zotto, Matteo Moglie 439

ID74 - Enhancing knowledge of engineering students at all levels on organic rankine cycle systems for their application in the built environment
Authors: Luca Cioccolanti, Ramin Moradi, Ermira Abdullah, Syamimi Saadon, Mohamad Yusof Idroas, Teoh Yew Heng, Kwanchai Kraitong 449

ID75 - Studying carbon dioxide and acetone mixtures in a single-stage absorption-compression cycle for heating and cooling applications
Authors: Jesús Gómez-Hernández, Ali Kholghi, Mercedes De Vega, Javier Villa, Ronan Grimes 458

ID77 - Valorising thermal composite recycling processes using Organic Rankine Cycles for combined heat and power applications
Authors: Ramin Moradi, Liu Yang 466

ID80 – Prediction of the ideal maximum operational temperature of hydrocarbon and HFCs as working fluids of Organic Rankine Cycle power plants based on transition state theory
Authors: Wei Yu, Chao Liu, Xijie Ban, Zhirong Li, Tianlong Yan 476

ID82 - Comparison of different evaporator topologies for industrial heat pumps
Authors: Sanjay Vermani, Nitish Anand, Johan Van Bael, Evgueni Touliankine, Aldo Serafino, Carlo De Servi. 486

ID83 - On the plant improvement of Solar-driven ORC based power unit for domestic microcogeneration
Authors: Fabio Fatigati, Marco Di Bartolomeo, Arianna Coletta, Diego Vittorini, Giammarco Di Giovine, Davide Di Battista, Roberto Cipollone 496

ID84 - Mapping the techno-economic potential of next-generation CSP plants running on transcritical CO2-based power cycles
Authors: Pablo Rodríguez-deArriba, Francesco Crespi, Sara Pace, David Sánchez 505

ID86 - Achieving 45% micro gas turbine efficiency through hybridization with Organic Rankine Cycles
Authors: Antonio Escamilla, David Sánchez Martínez, Lourdes García-Rodríguez 515

ID88 - Operational optimisation of the main heat rejection unit of CSP plants based on carbon dioxide mixtures
Authors: Francesco Crespi, Pablo Rodríguez-deArriba, Lourdes García-Rodríguez, David Sánchez. 525

ID89 - Mechanical design and rotor-dynamic analysis of the ORCHID turbine
Authors: Matteo Majer, Steven Chatterton, Ludovico Dassi, Alessio Secchiaroli, Edoardo Gheller, Carlo De Servi, Paolo Pennacchi, Piero Colonna, Matteo Pini 535

ID91 - Thermodynamic feasibility of a pumped thermal energy storage driven by ocean temperature gradient
Authors: Alessandra Ghilardi, Andrea Baccioli, Guido Francesco Frate, Lorenzo Ferrari 545

ID92 - Exergy-based methods for heat pumps
Authors: Mathias Hofmann, Jonas Freißmann, Malte Fritz, Jeremias H. Alexe, Francesco Witte, George Tsatsaronis 553

ID93 - Reduced order modelling of optimized heat exchangers for maximum mass-specific performance of Airborne ORC Waste Heat Recovery units
Authors: Fabio Beltrame, Dabo Krempus , Piero Colonna, Carlo De Servi. 563

ID97 - Basic design of an ORC demonstrator system for implementation in an Iron & Steel plant through the DECAGONE project
Authors: Magnus Windfeldt, Han Deng, Trond Andresen, Christopher Schifflechner 574

ID98 - Analytical estimation of the presence of non-condensable gases in the condensate tank of an Organic Rankine Cycle
Authors: Radheesh Dhanasegaran, Antti Uusitalo, Juha Honkatukia, Teemu turunen-Saaresti 584

ID101 - Advanced control of compressor inlet temperature in supercritical CO2 Brayton cycle
Authors: Rui Wang, Xuan Wang, Hua Tian, Gequn Shu. 596

ID103 - Potential for surplus-heat-to-power conversion in current and future aluminium production processes with off-gas recycling
Authors: Jonas Bueie, Magnus Windfeldt, Trond Andresen. 605

ID104 - Investigating the application range of ORC power plants for the exploitation of two-phase geothermal resources
Authors: Tristan Merbecks, Claudio Pietra, Paola Bombarda, Martin O. Saar, Paolo Silva, Dario Alfani. 615

ID109 - Cold Energy Recovery in LNG plants with Organic Rankine Cycle
Authors: Gabriele Marchiori, Marta Giudici, Giorgia Ruffato, Marco Astolfi 626

ID110 - Numerical investigation of organic vapor flow effects on a micro-scale radial turbocompressor
Authors: Andrés Sebastián, Rubén Abbas, Manuel Valdés 636

ID112 - Design, modeling and simulation of an experimental Rankine PTES system
Authors: Mario Petrollese, Giorgio Cau, Matteo Marchionni, Marcello Lorenzo Marroccu, Rosa Merchan 645

ID113 - Small-scale turbopumps for Waste Heat Recovery applications based on an Organic Rankine Cycles, modeling, analytical and experimental investigation
Authors: Sajjad Zakeralhoseini, Jürg Schiffmann 655

ID116 - Double-stage ORC system based on various temperature waste heat sources of the negative CO2 power plant
Authors: Kamil Stasiak, Pawel Ziólkowski, Dariusz Mikielewicz 665

ID117 - Optimization of organic Rankine cycle in ocean thermal energy conversion based on NSGA-II
Authors: Zheng Hu, Jiufa Chen, Bing Guo, Chengbin Zhang 679

ID118 - TES4Trig: Development of a demonstrator for the production of electricity, heating and cooling based on an Organic Rankine and an Ejector Cooling Cycle driven by high-temperature parabolic trough collectors with thermal energy storage
Authors: Konstantinos Braimakis, Dimitrios Tziritas, George Stavrakakis, Julio Terrón Gutiérrez, Siddhart Dutta, Christos Xynos, Panagiotis Zervas, Sotirios Karellas 689

ID119 - Simulation and operation of a CSP that works with a HRB Cycle
Authors: Antonio J. Subires, Antonio Rovira 701

ID123 - Towards a green energy community: integration of micro-ORCs combined with renewable energy technologies in buildings
Authors: Diego Antonio Rodríguez Pastor, Víctor Manuel Soltero Sánchez, Elisa Carvajal Trujillo, José Antonio Becerra, Ricardo Chacartegui 713

ID129 - Assessment of high temperature heat pump layouts equipped with a bladeless turboexpander
Authors: Matteo Passalacqua, Simone Maccarini, Stefano Barberis, Alberto Traverso 723

ID133 - Selection of the optimal working fluid in an Organic Rankine Cycle for Waste Heat Recovery through multi-objective optimization and decision making
Authors: Bipul Krishna Saha, El Mouatez Billah Messini, Syed J. Hoque, B Aneesh Bhat, Pramod Kumar 733

ID139 - Dual condensing pressure ORC for cryogenic energy storage
Authors: William M. Conlon, Milton J. Venetos 743

ID141 - Optimum coupling of thermal energy storage and power cycles for Carnot batteries
Authors: Salvatore Guccione, Rafael Guedez 751

ID142 - Aerodynamic design and numerical analysis of a counter-rotating centrifugal compressor
Authors: Cheikh Brahim Abed, Arthur Leroux 761

SEVILLE 2023
7th International Seminar on O.R.C. Power Systems

DOI: https://dx.doi.org/10.12795/9788447227457_30

NUMERICAL INVESTIGATION OF A TRANSONIC DENSE GAS FLOW OVER AN IDEALIZED BLADE VANE CONFIGURATION

A. Bienner[1,*], X. Gloerfelt[1], P. Cinnella[2], L. Hake[3] and S. aus der Wiesche[3]

[1] *Arts et Métiers, DynFluid Laboratory, 151 bd. de l'Hôpital, 75013 Paris, France.*
[2] *Sorbonne Univ., Jean Le Rond D'Alembert Institute, 4 place Jussieu, 75005 Paris, France.*
[3] *Muenster Univ. of Applied Sciences, Stegerwaldstr. 39, 48565 Steinfurt, Germany.*

*Corresponding author: aurelien.bienner@ensam.eu

ABSTRACT

A joint numerical and experimental investigation of an idealized blade vane configuration, representative of an ORC turbine, is undertaken using Novec649 as the working fluid. First laminar-turbulent transition over the blade is studied by means of large-eddy simulation (LES). The geometry of the leading edge is modified to avoid an incipient separation. Afterwards, RANS simulations are carried out for both air and Novec649. The dense gas flow achieves a lower pressure ratio and exit Mach number compared to air, while shock waves generated at the blade leading edge are weaker. However, the dense gas induces a lower base pressure resulting in higher losses. Qualitative and quantitative comparisons with experiments and with a wall-modeled LES are also planned.

1 INTRODUCTION

In most Organic Rankine Cycles (ORC), the working fluid, an organic compound, is compressed, heated, and then expanded in a turbine. The latter component can be critical for the cycle efficiency and it is of utmost importance to estimate the various loss mechanisms. Since ORC are intended to convert energy from relatively low-temperature sources, organic fluids are expanded in small-scale turbines, working in the transonic to supersonic regimes. At these flow speeds, the main losses in a linear cascade of turbine blades are due to shock-wave systems, laminar and turbulent boundary layers on blade walls and vortex shedding from the trailing edge (TE). Due to their molecularly complex structures, organic fluids operate in the so-called dense-gas regime, where the fundamental derivative of fluid dynamics is lower than one. A direct consequence is the decrease of the speed of sound during a compression, which would yield weaker shock waves, thus lower associated losses. On the contrary, the higher sound speed attained in the expansion fan close to the trailing edge would imply a lower base presssure, which can conversely increase the profile losses. Finally, little is known about the laminar-turbulent transition over ORC turbine blades. Designers generally assume a fully turbulent boudary-layer state but it is known that the transition will influence the viscous losses. Due to the combination of various mechanisms with a somehow contradictory influence, experimental and numerical databases are critical to improving turbine efficiency. Few facilities exist for dense gases and consist essentially in blowdown or suckdown tunnels, where only short-time statistics are possible (Baumgärtner *et al.*, 2020) A continuously running pressurized closed-loop wind tunnel (CLOWT) using Novec649, an environmentally friendly working fluid, in the high subsonic speed range, has been built at University of Muenster. Due to the high pressures and the high-density of Novec649, the experimental study of transonic linear cascade requires high compressor performance. As a consequence, the tunnel test section has relatively small dimensions and measurements for a linear cascade are thus challenging (Hake *et al.*, 2023). One way out is to use an idealized vane configuration. Instead of an entire blade cascade, the test set-up is usually limited to a single, geometrically simple blade with side-walls designed to generate quasi-periodic flow conditions. This idea has been used to study the transonic TE flow and the associated profile losses, e.g. by Denton & Xu (1990) or Rossiter *et al.* (2023). An idealized vane configuration with low-curvature blades has been designed in the work of Passmann (2021). A picture of the CLOWT test section is shown in figure 1, where the test section height $B = 36.5$mm. The experiments were conducted with air as the working medium in the outlet Mach number range 0.8 to 1.7, and included Schlieren visualizations, blade pressure distribution and traversing probe measurements. While the profile is lacking the curvature that most turbine blade profiles exhibit, it can be used as a test case for the investigation of basic phenomena such as tip gap flows in Passmann *et al.* (2018) or loss mechanisms with a dense gas in the present study.

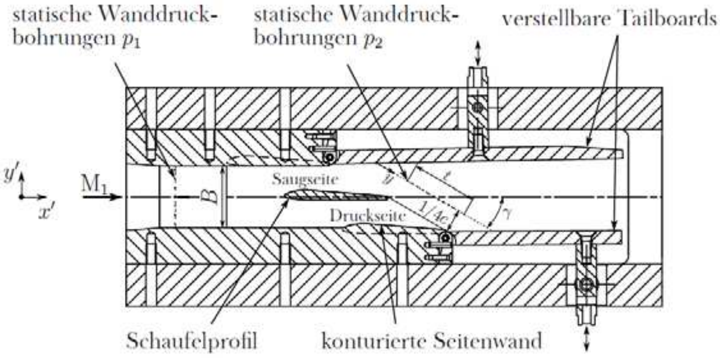

Figure 1: View (left) and sktech (right) of the experimental setup (from Passmann (2021).

194

Particular attention must be paid to the influence of the laminar-turbulent transition on turbine losses. Considering the high level of freestream turbulence (FST) intensity encountered in turbine environments, FST-induced transition is generally the principal mechanism of laminar-turbulent transition for turbine blades (Mayle, 1991; Sandberg & Michelassi, 2022). The Computational Fluid Dynamics (CFD) tools currently used in ORC design are based on Reynolds-averaged Navier-Stokes (RANS) models and usually ignore this phenomenon, considering that transition occurs straight downstream of blade leading edge (Romei *et al.*, 2020). To gain knowledge on FST-induced transition in dense-gas boundary layers (BL), a study was realized for a zero-pressure-gradient Novec649 BL by means of wall-resolved large eddy simulations (LES) (Bienner *et al.*, 2022*c*). It was found that, despite $M = 0.9$ in the freestream, the turbulent profiles were very close to incompressible databases due to the high specific heat of Novec649, which significantly reduces friction heating. Moreover, the large-scale FST was shown to influence not only the location of transition but also its mechanism, notably the laminar streaks size and arrangement. To investigate the effect of a finite thickness leading edge and of the favorable pressure that it induces on FST-induced transition, LES have been performed around the leading edge of our idealized turbine stator (Bienner *et al.*, 2022*b*). It was shown that transition occurs early on the blade and that the laminar-streak breakdown, which is usually the precursor of turbulent spots, is highly disrupted by large vortical structures impinging the leading edge. In the present paper, additional results on the leading edge study are presented, showing the influence of the geometry over the transition. Afterwards, the flow of Novec649 past the complete idealized blade is investigated using RANS, due to the extremely high cost of LES. A comparison with air flow in the same conditions is used to get insights into dense-gas effect on turbine efficiency. Companion experiments are scheduled for June/July 2023, and we plan to present them at the conference. High-fidelity wall-modeled LES are also planned.

M_{in}	c_{in} [m/s]	p_{in} [bars]	p_{in}/p_c	T_{in} [°C]	T_{in}/T_c	ρ_{in} [kg/m^3]	ρ_{in}/ρ_c	μ_{in} [Pa.s]	Γ_{in}
0.52	74	3.3	0.17	60	0.75	44.1	0.07	1.26×10^{-5}	0.8

Table 1: Thermodynamic and aerodynamic conditions at the inlet of LES domain. Subscript *in* is used for inlet quantities and subscript *c* for critical ones.

2 NUMERICAL SET-UP

The in-house code MUSICAA is used to solve the compressible Navier-Stokes equations over a curvilinear multiblock domain using generalized coordinate transformation. The fluid Novec649 is modeled with the Peng-Robinson-Stryjek-Vera equation of state (Stryjek & Vera, 1986) and the Chung-Lee-Starling model (Chung *et al.*, 1988) for transport properties. The ideal gas law and Sutherland's model are used for air flows. Concerning LES of the leading-edge region (§ 3), spatial discretization uses 10th-order centered finite differences for inviscid fluxes and 4th-order schemes for viscous fluxes, supplemented by a 10th-order selective filtering. A four-stage Runge-Kutta (RK4) algorithm is used for time integration and a fourth-order implicit residual smoothing (IRS) (Bienner *et al.*, 2022*a*) is applied to enlarge its stability limit and enable larger timesteps. Non-reflecting Tam & Dong's boundary conditions are applied at the inlet, top and outflow boundaries with imposed mean quantities from a companion RANS simulation. A sponge zone combining grid stretching and a Laplacian filter is added at the oulet. At the inlet, synthetic freestream turbulence is generated by means of Random Fourier Modes. Adiabatic no-slip conditions are applied at the wall and periodicity is enforced in the spanwise direction. More details can be found in Bienner *et al.* (2022*b*). For RANS simulations (§ 4), the Spalart-Allmaras model is used, with a turbulent viscosity prescribed at the inlet $\tilde{\nu} = 10\nu_\infty$. The RANS transport equation is discretized on a 3-point stencil, whereas 4th-order standard centered differences are used for the inviscid and viscous fluxes combined with a 4th-order Jameson-type selective filtering. As the repeated application of the filter can lead to an overdissipation for small time steps (or CFL numbers), the filtering coefficient χ is replaced by min(χ,CFL) (Edoh *et al.*, 2018), so that the shocks are sharply captured in steady computations. The RK4 algorithm is supplemented with a second-order IRS. Stagnation pressure and temperature are imposed at the inlet, based on Riemann invariants, whereas a back-pressure condition is used at the outlet. Adiabatic no-slip wall conditions are used.

3 INFLUENCE OF THE GEOMETRY ON LAMINAR-TURBULENT TRANSITION

To get insights into the laminar-turbulent transition for the idealized vane configuration, we performed LES on a subregion of the turbine vane centered around the suction side of the LE. Operating conditions are representative of the future experimental campaign in CLOWT facility (see table 1), corresponding to a flow of Novec649 in relatively dilute conditions. More details about the thermodynamic conditions are given in section 4.2, along with results concerning the Novec649 RANS simulation that served to initialize and to impose boundary conditions mean values in LES. The fundamental derivative of gas dynamics Γ has a value below 1 so that the flow occurs in the so-called dense-gas thermodynamic region, as used in ORC applications. In a first attempt, we used the idealized blade geometry of Passmann (2021), which was used to investigate tip gap effects on losses in the CLOWT facility (using air as the working fluid). The profile consists of simple circular arcs and straight lines. The rear parts of pressure and suction side are composed of straight lines. The suction side is inclined at an angle of 4.5° with respect to the pressure side. The chord length of the profile is set at *ch*=62 mm and a thick rounded TE shape was chosen (diameter of 2.4 mm). This leads to high Reynolds conditions, with $Re_{ch,in} = 9 \times 10^6$ with Novec649. The flow accelerates from $M = 0.5$ up to $M = 1.1$ at the outlet. The incoming FST has an intensity $T_u = \sqrt{(u'^2 + v'^2 + w'^2)/3} = 5\%$ and a Reynolds number $Re_{L_f} = 18 \times 10^3$, based on the turbulence integral length-scale L_f. A computational

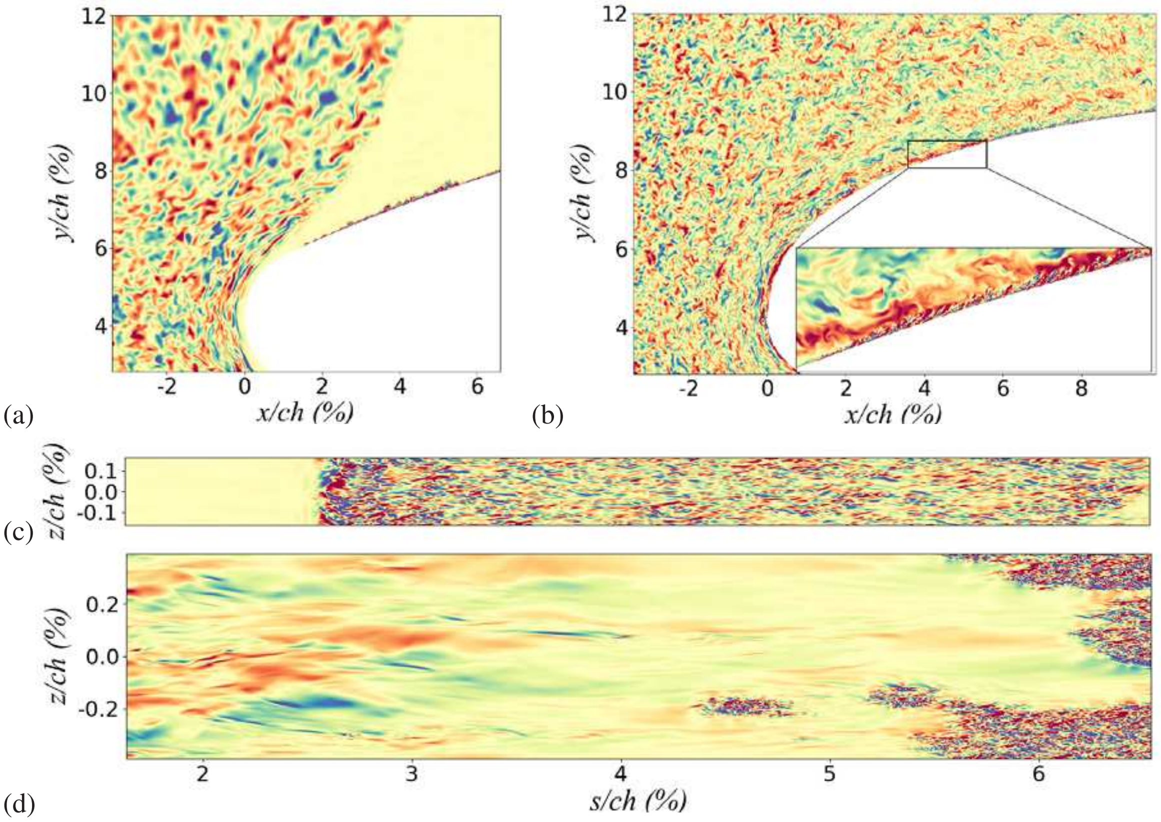

Figure 2: Snapshot of the spanwise fluctuations w' in a mid-span (a-b) and a wall-normal plane at $n^+ \sim 10$ (c-d) for the original (a-c) and smoothed (b-d) geometry. Levels: $\pm 0.05 \times c_{in}$

196

domain of 350 millions points was used, with a resolution $\Delta n_w^+ \times \Delta s^+ \times \Delta z^+ \sim 0.3 \times 25 \times 10$, where s and n denote the curvilinear abscissa along the blade and the wall-normal distance, respectively (Δn_w^+ being the resolution at the wall). Snapshots in mid-span and wall-normal planes are displayed in figures 2(a) and (c). FST has not yet impacted the leading-edge that the transition has already occurred on the suction side, meaning that the transition is not induced by the FST. The early turbulent front at $s = 1.5$ mm, which is clearly identified on the wall-normal slice, results from an incipient flow separation occuring at a curvature discontinuity resulting from the connection of two circles forming the idealized blade geometry.

In turbines, the most likely mechanism of laminar-turbulent transition is the FST-induced transition. Since we are interested in designing an idealized configuration representative of ORC turbines, a new geometry of the LE region is proposed to avoid the curvature discontinuity responsible for the laminar-separation-bubble transition. The curvature evolution is smoothed using two super-ellipses defined by $(\frac{a-x}{a})^n + (y/b)^n = 1$ (Narasimha & Prasad, 1994), where $n = 2.3$, $a/ch = 18.47\%$, $b/ch = 5.81\%$ for the suction side super-ellipse and $n = 2.4$, $a/ch = 26.70\%$, $b/ch = 4.18\%$ for the pressure side super-ellipse. Then, the suction side straight line is connected to the super-ellipse using a Bézier curve. The trailing-edge (TE) of the smoothed geometry is kept equal to the initial one. The original and smoothed nose geometries are compared in figure 3, the smoothed one being closer to the typical shape of turbine stator noses. The curvature discontinuity of the original design is visible in the right insert. Note that the pressure distribution on the blade is weakly affected. A new LES is carried out on a refined grid of 2.1 billions points, which yields a resolution $\Delta n_w^+ \times \Delta s^+ \times \Delta z^+ \sim 0.45 \times 13 \times 11$, typical of wall-resolved LES. The inlet turbulence corresponds to $T_u = 5\%$ and $Re_{L_f} = 11 \times 10^3$. Spanwise velocity snapshots in figure 2(b)-(d) show the transitional front is no longer localized but is distributed along a transitional region where turbulent spots appear and merge to form the turbulent BL, as expected in a FST-induced transition. Further analyses of the LES results on the smoothed geometry can be found in Bienner *et al.* (2022*b*). An important conclusion is that the FST-induced transition occurs rapidly at approximately 6% of the chord, despite the favorable pressure gradient, which can delay significantly the transition location (Mayle, 1991). It also justifies the use of RANS simulations without any transition model in the following.

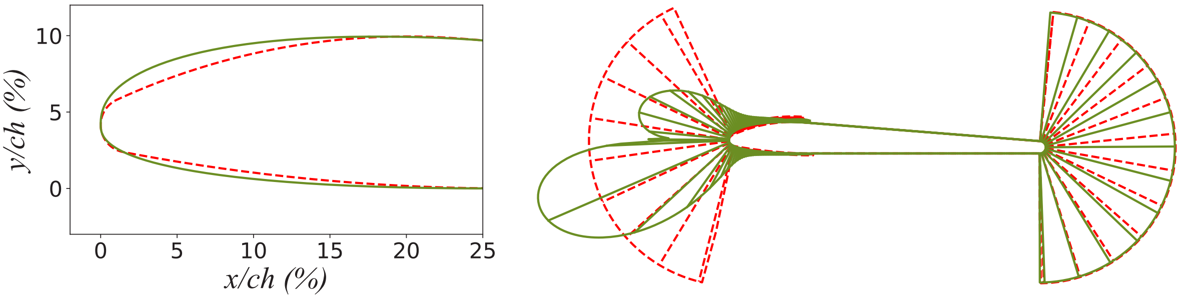

Figure 3: Comparison of the original (- - -) and smoothed (——) geometries: zoom on the LE region (left) and profile curvature (right).

4 PRELIMINARY STUDIES OF THE IDEALIZED TURBINE BLADE

4.1 Validation of the RANS strategy for air flow

To assess our RANS methodology, the experimental investigation with air in Passmann (2021) is numerically reproduced (the LE geometry is thus the original one). The 2D computational grid of 234×10^3 points has a resolution $\Delta n_w^+ \sim 1.0 - 1.2$ and $\Delta s/ch \sim 0.30\%$, with 720 points along the blade. The domain is extended 1.5 chord upstream of the LE and 2 chords downstream of the TE. At the inlet, a total pressure of $p_{0,1} = 4$ bars and a total temperature of $T_{0,1} = 308$ K are imposed. A comparison of the shock system in the TE region with an experimental Schlieren picture is proposed in figure 4. The numerical simulation correctly reproduces the fishtail shock system and the position of the oblique shock waves. Moreover, the pressure distribution along the blade in figure 4 (right) is also in good agreement with the experimental one. To check the grid convergence, RANS is also run on a finer mesh, with $\Delta s/ch \sim 0.22\%$ and 900 points along the blade. The pressure distribution perfectly matches the medium grid one, showing that mesh independency is achieved on the medium grid. 197

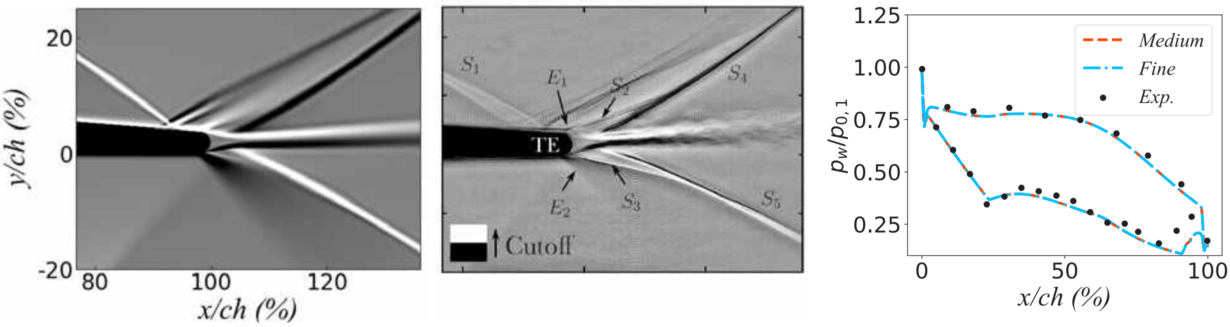

Figure 4: Schlieren visualizations of the shock system in RANS (left) and Passmann's experiment (middle). Right: pressure distribution around the blade from experiments and RANS simulations.

Case	ch	M_1	c_1	$p_{0,1}$	$T_{0,1}$	$\rho_{0,1}$	M_2	c_2	Re_{M_2}	π
	$[mm]$		$[m/s]$	[bars]	$[K]$	[kg/m^3]		$[m/s]$		$p_{0,1}/p_2$
Novec649	61.2	0.55	76	3.8	335	55.0	1.59	87	8.5×10^6	3.7
Air	246	0.51	343	4.0	308	4.52	1.71	279	8.5×10^6	5.3

Table 2: Thermodynamic and aerodynamic conditions of RANS simulations.

4.2 Dense-gas effects

As already mentioned, the thermodynamic conditions selected for Novec649 correspond to relatively dilute conditions, with a total pressure of $p_{0,1} = 3.8$ bars and a total temperature of $T_{0,1} = 335$ K (see table 2). The inlet values are calculated one chord upstream of the LE and the exit values are evaluated along the line of measure plotted in figure 5, which corresponds to a distance of $0.25 \times ch/\cos(\gamma)$ where $\gamma = 60°$ denotes the stagger angle. The outlet Reynolds number Re_{M_2}, based on the chord and the outlet Mach number M_2, is equal to 8.5×10^6. Several regions of interest are identified in the Schlieren-like visualization of figure 5: laminar-turbulent transition (region 1), shock-wave-boundary layer interactions (region 2) and wake development (region 3).

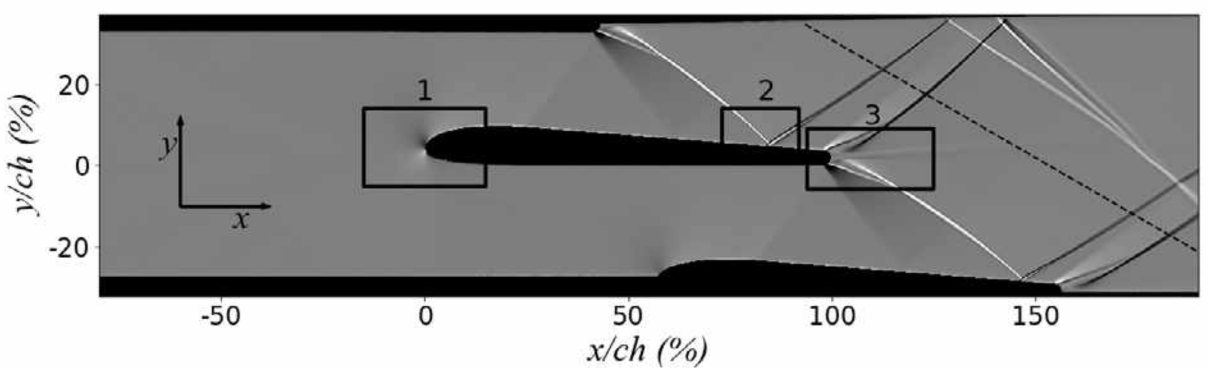

Figure 5: Schlieren-like visualization of the idealized blade vane configuration in the Novec649 2D RANS simulation (see section 4.2): density gradient in y-direction (levels $\pm 10^4$). – – –: line of measure.

198

For comparison purposes, a simulation with air is also realized. The chord is modified to 246 mm in order to match the outlet Reynolds number of the Novec649 simulation and the newly designed nose is used (see table 2). First, we observe that the pressure ratio, $\pi = p_{0,1}/p_2$, is significantly lower in the Novec649 configuration ($\pi_{Novec649} = 3.7$) than in air ($\pi_{air} = 5.3$). To get more insights, the pressure distributions of the air and Novec simulations are compared in figure 6 (left). Concerning the air flow, the pressure distribution of the smoothed blade profile is rather similar to the one of the initial blade profile in figure 4 (right), as already mentioned in section 3. In line with the differences observed in pressure ratio, the pressure distribution levels around the blade for the Novec649 simulation are increased, which would correspond to a decrease of the isentropic Mach number. Moreover, a difference in the position of the reflected shock at the suction side is noticed. The fundamental derivative of gas dynamics $\Gamma = 1 + \frac{\rho}{c} \frac{\delta c}{\delta \rho}_s$, shown in figure 6 (right), increases from 0.8 upstream to 0.95 downstream but stays below 1.0, meaning that the flow occurs inside the dense-gas region. This results in a reverse behavior of the speed of sound compared to perfect gases, namely, $\frac{\delta c}{\delta \rho}_s < 0$ and the speed of sound increases while the flow expands. For instance, in the shock interaction region in figure 7, the speed of sound increases from 76 at the inlet to 90 at the outlet in the Novec649 flow whereas, in the air configuration, c decreases monotonically. This yields a lower Mach number increase in the Novec flow than in the air flow (see figure 8). Therefore, shock waves are weakened in the dense gas yielding a lower pressure ratio. In particular, the higher pressure ratio across the impinging shock on the suction side in the air flow induces a larger separation bubble compared to the Novec649 flow (see figure 9). The second compression shock at the impingement, hardly noticeable in the dense gas configuration, is clearly visible in air. Due the larger separation region and the fact that the location of the shock is closer to the TE in the air flow, the BL remains separated at the TE downstream whereas it is attached in the Novec649 flow. Finally, due to the acceleration around the TE corner, the flow undergoes a supersonic expansion before separating from the TE. At the end of the recirculation region, the supersonic flow coming from the suction and pressure sides re-aligns by means of a fish-tail shaped system of shock waves. Due to the differences in the BL states and in the expansion around the TE, the opening angle of the fishtail shocks is increased with Novec649.

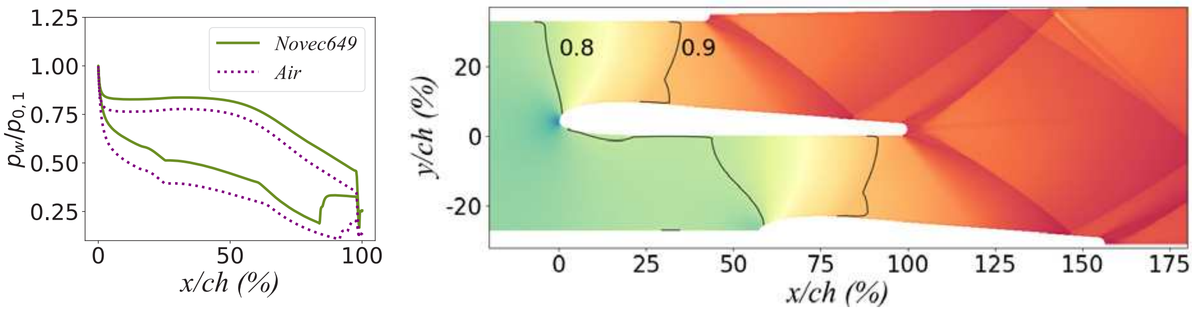

Figure 6: Left: pressure distribution of the Novec649 and air RANS simulation around the smoothed profile. Right: Γ field in the Novec649 RANS simulation (levels 0.7 to 1.0).

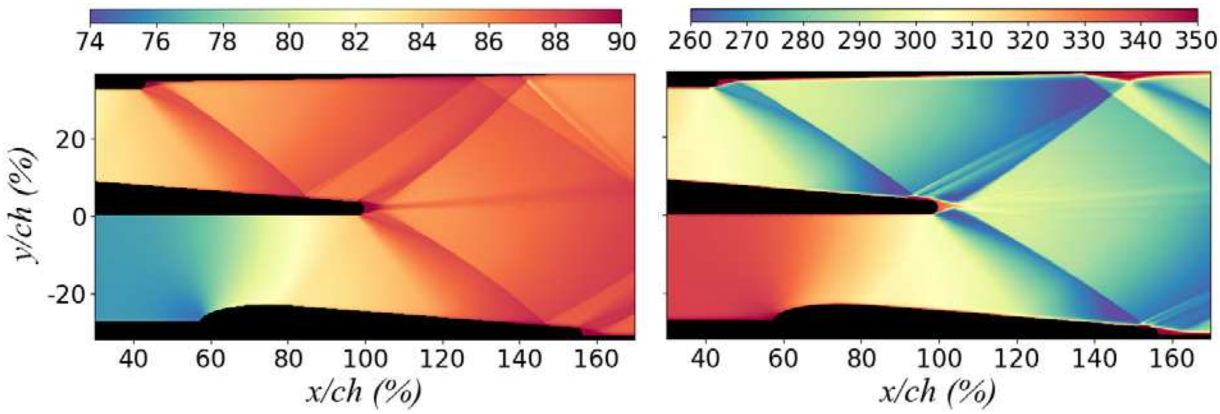

Figure 7: Sound speed c field of the Novec649 (left) and air (right) RANS simulation around the smoothed profile (levels 0.4 to 2.0).

5 CONCLUSION AND FUTURE WORK

The transonic dense gas flow over an idealized blade vane configuration has been studied by means of RANS simulations. When compared to air flow at similar Reynolds number conditions, the investigation reveals that the Novec649 flow exhibits weaker shocks due to the reverse behavior of the sound speed, ultimately leading to a lower pressure ratio between inlet and outlet. The shock topology is consequently affected, with a wider opening angle of the fishtail shocks in the Novec649 configuration. Moreover, the fact that the shock impingement in Novec649 arises more upstream of the TE with respect to air changes significantly

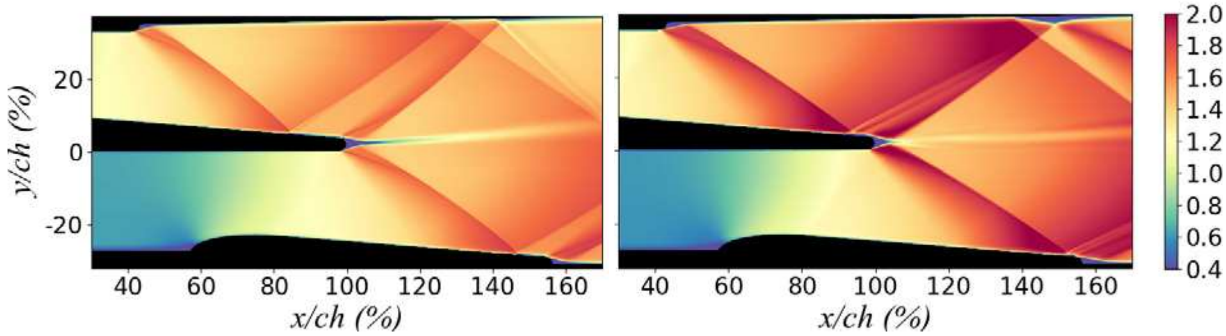

Figure 8: Mach number field of the Novec649 (left) and air (right) RANS simulation around the smoothed profile (levels 0.4 to 2.0).

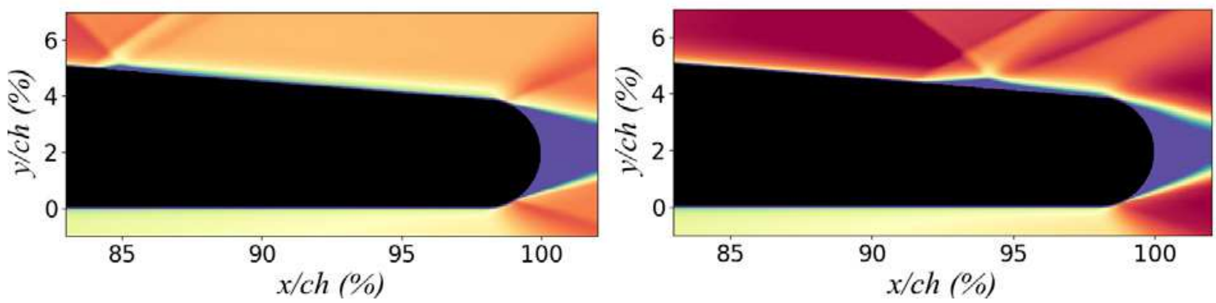

Figure 9: Mach number field of the Novec649 (left) and air (right) RANS simulation (levels 0.4 to 2.0): zoom on the shock-BL interaction and on the TE.

the shock-BL interaction and the BL state at the wake birth, which may affect the wake development. In particular, unsteady RANS captures the vortex shedding in the wake for the air flow whereas a steady wake is obtained in Novec649. This is a pitfall of RANS modeling, notoriously inaccurate for the prediction of several phenomena occurring in turbomachinery. For instance, RANS simulations cannot predict accurately the wake dynamics or fails in capturing shock-BL interaction dynamics, overestimating the shock strength while underestimating the size of separated region eventually occurring at the shock foot. We plan to perform high-fidelity simulations on the idealized blade configuration to investigate the complex dynamics in the wake vicinity. Due to the high Reynolds number based on the chord of the profile ($Re_{ch} \sim 10 \times 10^6$), a direct numerical simulation (DNS) or a wall-resolved LES is out of reach. Indeed, as seen in section 3, 2.1 billions points are necessary to simulate only $\sim 10\%$ of chord on the suction side, which leads to almost 40 billions in order to simulate the full blade. Therefore, the LES will be conducted with wall-model to relax the constraint on the near wall resolution but also to be able to significantly increase the timestep. Since we observed that the boundary layer becomes turbulent relatively rapidly, the use of wall-modeled LES is specially relevant to reduce the computational cost.

Even if weaker shocks are encountered with Novec649, the overall losses will not necessarily be lower. Indeed, the profile losses associated with the base pressure at the TE are expected to increase with dense gases. The wall-modeled LES will allow a proper description of the wake dynamics and thus a detailed analysis of the TE loss mechanisms. A comparison with air will be realized in order to quantify the effect of the dense gas on the turbine performance (Baumgärtner *et al.*, 2020) and on the energy separation phenomenon (Sieverding & Manna, 2020). The companion experiments will provide a quantitative and qualitative comparison with the numerical simulations, thanks to Schlieren imaging, pressure distribution around the blade and pressure/velocity profiles in the blade wake.

ACKNOWLEDMENTS

This research has been funded by the Agence Nationale de la Recherche through the ANR-20-CE92-0019-02 project Regal-ORC. This work was granted access to the HPC resources of IDRIS and TGCC under the allocation A0132A01736 made by GENCI (Grand Equipement National de Calcul Intensif).

References

BAUMGÄRTNER, D., OTTER, J.J. & WHEELER, A.P.S. 2020 The effect of isentropic exponent on transonic turbine performance. *ASME Journal of Turbomachinery* **142** (8), 081007.

BIENNER, A., GLOERFELT, X. & CINNELLA, P. 2022*a* Assessment of a high-order implicit residual smoothing time scheme for multiblock curvilinear meshes. *11th International Conference on Computational Fluid Dynamics (ICCFD11)* 11-15 July, Maui, HI, USA .

BIENNER, A., GLOERFELT, X. & CINNELLA, P. 2022*b* Leading-edge effects in freestream turbulence induced transition in a dense gas flow. *13th Direct and Large-Eddy Simulations (DLES13)* 26-28 October, Udine, Italy .

BIENNER, A., GLOERFELT, X., CINNELLA, P., HAKE, L., AUS DER WIESCHE, S. & STREHLE, S. 2022*c* Study of bypass transition in dense-gas boundary layers. *12th International Symposium on Turbulence and Shear Flow Phenomena Conference (TSFP12)* 19-22 July, Osaka, Japan (Online) .

CHUNG, T.H., AJLAN, M., LEE, L.L. & STARLING, K.E. 1988 Generalized multiparameter correlation for nonpolar and polar fluid transport properties. *Ind. Eng. Chem.* **27** (4), 671–679.

DENTON, J.D. & XU, L. 1990 The trailing edge loss of transonic turbine blades. *ASME Journal of Turbomachinery* **112**, 277–285.

EDOH, A.K., MUNDIS, N.L., MERKLE, C.L., KARAGOZIAN, A.R. & SANKARAN, V. 2018 Comparison of artificial-dissipation and solution-filtering stabilization schemes for time-accurate simulations. *J. Comput. Phys.* **375**, 1424–1450.

HAKE, L., SUNDERMEIER, S., AUS DER WIESCHE, S., MATAR, C., CINNELLA, P. & GLOERFELT, X. 2023 Investigation of the turbulence level and the vortex shedding in a turbine cascade working with an organic vapor at subsonic Mach numbers. In *7^{th} International Seminar on ORC Power Systems (ORC2023)*. Seville, Spain.

MAYLE, R.E. 1991 The role of laminar-turbulent transition in gas turbine engines. In *Proceedings of ASME International Gas Turbine and Aeroengine Congress and Exposition*. Orlando, USA.

NARASIMHA, R. & PRASAD, S. N. 1994 Leading edge shape for flat plate boundary layer studies. *Experiments in Fluids* **17**, 358–360.

PASSMANN, M., AUS DER WIESCHE, S. & JOOS, F. 2018 An experimental and numerical study of tip-leakage flows in an idealized turbine tip gap at high Mach numbers. In *ASME Turbomachinery Technical Conference and Exposition*, , vol. GT2018-76366. Oslo, Norway.

PASSMANN, M. G. 2021 Experimentelle Untersuchungen zu transsonischen Schaufel-Spaltströmungen in Axialturbinen. PhD thesis, Münster University.

ROMEI, A., VIMERCATI, D., PERSICO, G. & GUARDONE, A. 2020 Non-ideal compressible flows in supersonic turbine cascades. *J. Fluid Mech.* **882**, A12–1–A12–26.

ROSSITER, A.D., PULLAN, G. & MELZER, A.P. 2023 The influence of boundary layer state and trailing edge wedge angle on the aerodynamic performance of transonic turbine blades. *ASME Journal of Turbomachinery* **145**, 041008.

SANDBERG, R.D. & MICHELASSI, V. 2022 Fluid dynamics of axial turbomachinery: blade and stage-level simulations and models. *Ann. Rev. Fluid Mech.* **54**, 255–285.

SIEVERDING, C. & MANNA, M. 2020 A review on turbine trailing edge flow. *International Journal of Heat and Fluid Flow* **5** (2), 1–60.

STRYJEK, R. & VERA, J.H. 1986 PRSV: An improved Peng-Robinson equation of state for pure compounds and mixtures. *The Canadian Journal of Chemical Engineering* **64** (2), 323–333.

This book contains the compilation of works contributed to the *7th International Seminar on Organic Rankine Cycle Power Systems* (ORC 2023), held in Seville between the 4th and 6th of September 2023. The event was hosted by Universidad de Sevilla on behalf of the Knowledge Centre on Organic Rankine Cycle Technology (KCORC), incorporated in The Netherlands.

The ORC conference, organized biennially, stems as the only conference that is specific to ORC technology, therefore gathering a diverse community whose affiliation spans across all the interested stakeholders, not only in this particular technology but also and in a broader context, in the energy transition. Original equipment manufacturers, professional associations, end-users, investors, policy makers, academics, scientists feel at home at ORC 2023.

The almost 100 proceedings in this book cover a wide variety of topics, from fundamentals to system integration through component design, accounting for thermodynamic performance as well as component design. In addition to this, and as a new track in 2023, works on heat pump technology were also accepted in order to raise awareness of the strong ties between both technologies, specifically in energy storage applications.

This book provides an excellent overview of the current maturity of power systems based on Organic Rankine Cycle technology for applications as diverse as geothermal and waste heat recovery in industry or downstream of other prime movers (e.g., marine applications). It is also an excellent source of information to understand the current challenges faced by the technology, stemming from a very competitive market and increasingly stringent environmental regulations.

The organizers of ORC 2023 hope that the reader finds this work as exciting as the attendees to the conference and, maybe, make the decision to join the 8th edition to the conference in 2025.

KCORC
KNOWLEDGE CENTER
ORGANIC RANKINE CYCLE

eus EDITORIAL
UNIVERSIDAD DE SEVILLA